

Tunable artificial plasmonic nanolaser with wide spectrum emission operatingat room temperature

Peng Zhou(周鹏), Jia-Qi Guo(郭佳琦), Kun Liang(梁琨), LeiJin(金磊), Xiong-Yu Liang(梁熊玉), Jun-Qiang Li(李俊强), Xu-Yan Deng(邓绪彦), Jian-Yu Qin(秦建宇), Jia-Sen Zhang(张家森), and Li Yu(于丽)

Citation: Chin. Phys. B, 2024, 33 (**5**): 054210. DOI: 10.1088/1674-1056/ad2dca
Journal homepage: http://cpb.iphy.ac.cn; http://iopscience.iop.org/cpb

What follows is a list of articles you may be interested in

Giant and controllable Goos—Hänchen shift of a reflective beam off a hyperbolic metasurface of polar crystals

Tian Xue(薛天), Yu-Bo Li(李宇博), Hao-Yuan Song(宋浩元), Xiang-Guang Wang(王相光), Qiang Zhang(张强), Shu-Fang Fu(付淑芳), Sheng Zhou(周胜), and Xuan-Zhang Wang(王选章)
Chin. Phys. B, 2024, 33 (**1**): 014207. DOI: 10.1088/1674-1056/acdac2

Active control of surface plasmon polaritons with phase change materials

Yuan-Zhen Qi(漆元臻), Qiao Jiang(蒋瞧), Hong Xiang(向红), and De-Zhuan Han(韩德专)
Chin. Phys. B, 2023, 32 (**10**): 104202. DOI: 10.1088/1674-1056/accd5a

Independently tunable dual resonant dip refractive index sensor based on metal—insulator—metal waveguide with Q-shaped resonant cavity

Haowen Chen(陈颢文), Yunping Qi(祁云平), Jinghui Ding(丁京徽), Yujiao Yuan(苑玉娇), Zhenting Tian(田振廷), and Xiangxian Wang(王向贤)
Chin. Phys. B, 2022, 31 (**3**): 034211. DOI: 10.1088/1674-1056/ac48fe

Mode splitting and multiple-wavelength managements of surface plasmon polaritons in coupled cavities

Ping-Bo Fu(符平波) and Yue-Gang Chen(陈跃刚)
Chin. Phys. B, 2022, 31 (**1**): 014216. DOI: 10.1088/1674-1056/ac0e28

Bound states in the continuum on perfect conducting reflection gratings

Jianfeng Huang(黄剑峰), Qianju Song(宋前举), Peng Hu(胡鹏), Hong Xiang(向红), and Dezhuan Han(韩德专)
Chin. Phys. B, 2021, 30 (**8**): 084211. DOI: 10.1088/1674-1056/abeee4

Tunable artificial plasmonic nanolaser with wide spectrum emission operating at room temperature

Peng Zhou(周鹏)[1], Jia-Qi Guo(郭佳琦)[2], Kun Liang(梁琨)[1], Lei Jin(金磊)[1], Xiong-Yu Liang(梁熊玉)[1], Jun-Qiang Li(李俊强)[1], Xu-Yan Deng(邓绪彦)[1], Jian-Yu Qin(秦建宇)[1], Jia-Sen Zhang(张家森)[2,3], and Li Yu(于丽)[1,†]

[1] *State Key Laboratory of Information Photonics and Optical Communications, School of Science, Beijing University of Posts and Telecommunications, Beijing* 100876, *China*

[2] *State Key Laboratory for Artificial Microstructures and Mesoscopic Physics, School of Physics, Peking University, Beijing* 100876, *China*

[3] *Peking University Yangtze Delta Institute of Optoelectronics, Peking University, Nantong* 226010, *China*

(Received 28 December 2023; revised manuscript received 20 February 2024; accepted manuscript online 28 February 2024)

With the rapid development of information and communication technology, a key objective in the field of optoelectronic integrated devices is to reduce the nano-laser size and energy consumption. Photonics nanolasers are unable to exceed the diffraction limit and typically exhibit low modulation rates of several GHz. In contrast, plasmonic nanolaser utilizes highly confined surface plasmon polariton (SPP) mode that can exceed diffraction limit and their strong Purcell effect can accelerate the modulation rates to several THz. Herein, we propose a parametrically tunable artificial plasmonic nanolasers based on metal–insulator–semiconductor–insulator–metal (MISIM) structure, which demonstrates its ability to compress the mode field volume to $\lambda/14$. As the pump power increases, the proposed artificial plasmonic nanolaser exhibits 20-nm-wide output spectrum. Additionally, we investigate the effects of various cavity parameters on the nanolaser's output threshold, offering potentials for realizing low-threshold artificial plasmonic nanolasers. Moreover, we observe a blue shift in the center wavelength of the nanolaser output with thinner gain layer thickness, predominantly attributed to the increased exciton–photon coupling strength. Our work brings inspiration to several areas, including spaser-based interconnects, nano-LEDs, spontaneous emission control, miniaturization of photon condensates, eigenmode engineering of plasmonic nanolasers, and optimal design driven by artificial intelligence (AI).

Keywords: surface plasmon polaritons, nanolaser, ultrafast, MISIM

PACS: 42.55.Px, 68.47.Fg, 52.25.Os, 81.07.Gf **DOI:** 10.1088/1674-1056/ad2dca

1. Introduction

The rapidly expanding information and communication technology (ICT) is revolutionizing people's lives. The exponential growth of ICT services has led to an increasing demand for efficient data processing, storage, and communication systems.[1] The shift from electrical to optical interconnections has been greatly advanced by the inherent bandwidth advantages of optical communications. For instance, vertical cavity surface emitting lasers (VCSELs) have found widespread applications in data centers, supercomputers, and LIDAR systems.[2] However, traditional photonics devices continue to face challenges such as large feature sizes, limited speed, and high energy consumption.[3–5] In recent years, there has been a surge of interest in plasmonic nanolasers due to their exceptional physical properties. These nanolasers exhibit strong near-field localization, surpassing the diffraction limit and compressing the mode-field volume to $(100/\lambda^2)$.[6–8] Additionally, they benefit from enhanced spontaneous radiation through the high Purcell effect.[9,10] Theoretically, plasmonic nanolasers can be directly modulated by using sub-100-fs pulse widths under electric pumping.[11–13] These nanolasers hold immense potential for applications in future data centers and on-chip optical interconnect systems.

In this work, we propose an MISIM-structured artificial plasmonic nanolaser. The proposed nanolaser configuration enables the mode field volume to be compressed to $\lambda/14$, with only a 12-μm cavity length. We conduct a comprehensive investigation by fabricating numerous artificial equipartitioned exciton microcavities to analyze the influence of different cavity parameters on the nanolaser threshold. Our findings reveal that reducing the thickness of the CdSe nanobelt leads to a blue-shift in the center wavelength of output, primarily attributed to exciton–photon coupling strength increasing due to reduction in gain layer size.[14,15] Furthermore, we observe wide spectrum output characteristics in the proposed nanolasers as the pump power increases. This observation sheds light on the intrinsic eigenmode control in the excited radiation process of a plasmonic nanolasers. We believe that our proposed plasmonic nanolaser has significant applications in optical interconnection, near-field spectroscopy and sensing, as well as far-field beam synthesis through near-field techniques.

†Corresponding author. E-mail: yuliyuli@bupt.edu.cn

© 2024 Chinese Physical Society and IOP Publishing Ltd

2. Experiment

CdSe nanobelts are synthesized by a chemical vapor deposition (CVD) method using CdSe powder with purity of 99.99% as effective impurity source.[16–18] The substrate for growing film is a magnetron sputter coated 10-nm-thick Si substrate. Figure 1(a) shows the color variation of CdSe nanobelts with different thickness, observed under an optical microscope. The values of thickness and width of these nanobelts are influenced by growth temperature, growth time, and Ar gas flow rate. Provided that all other conditions are controlled, longer growth time leads to an increase in the thickness of the nanobelts. Figure 1(b) shows a three-dimensional (3D) model of a thicker CdSe nanobelt obtained through AFM characterization. The scan confirms the uniform thickness of our grown nanobelts, with several randomly selected nanobelts exhibiting a surface uniformity within 3 nm. The scan along the white line in Fig. 1(c) indicates an about 170-nm-thick CdSe nanobelt. Figure 1(d) displays the TEM pattern of another CdSe nanobelt at a magnification of 10^4 times, while figure 1(e) reveals a clear single-crystal arrangement at a magnification of 8×10^5 times. This observation confirms the high quality of the grown CdSe nanobelts. Additionally, figure 1(f) illustrates the components of the grown CdSe nanobelt, demonstrating the absence of impurities. After normalization, the ratio of Cd to Se is approximately 1 to 1. The C content in the figure comes from the influence of the carbon supported film on the copper mesh. These findings support the conclusion that our nanobelts are of superior quality.

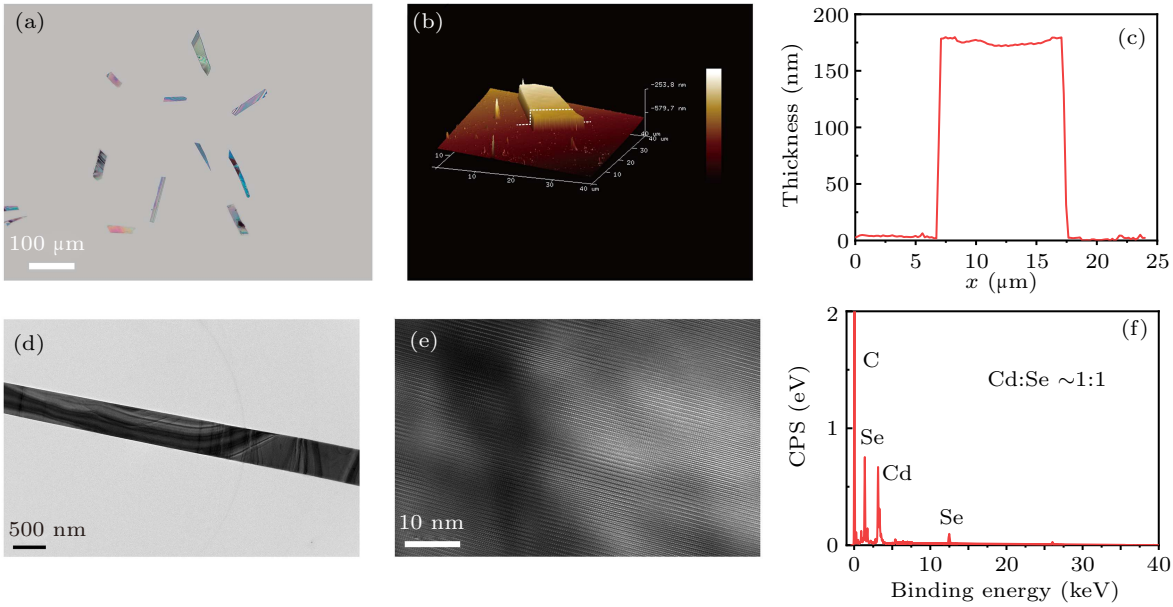


Fig. 1. Characterization of CdSe nanobelts. (a) Optical photograph showing the CdSe nanobelts samples with different thicknesses. Scale bar is 100-μm long. (b) 3D schematic diagram of CdSe nanobelt samples in AFM. (c) Scanning the CdSe nanobelt along the white line in panel (b), which demonstrates that the thickness is about 170 nm and the width is about 10 μm. (d) TEM image at a magnification of 10^4 times. Scale bar is 500-nm long. (e) TEM image at a magnification of 8×10^5 times, which suggests that CdSe nanobelts exhibits a strict single-crystal arrangement. Scale bar is 10-nm long. (f) EDS spectra of CdSe nanobelts.

Utilizing high-quality CdSe nanobelts, we develop a metal–insulator–semiconductor–insulator–metal (MISIM) structured Fabry–Perot (FP) cavity. Artificial plasmonic microcavities with varying structural parameters can be etched by using a focused ion beam (FIB). The fabrication procedure for the artificial FP cavity is as follows: (i) sequential deposition of an 18-nm-thick Au film and a 6-nm-thick MgF_2 film onto one side of the SiC substrate by using magnetron sputtering; (ii) transferring the CdSe nanobelt dispersed on silicon wafers onto the surface of the MgF_2 film by using a microswitching system; (iii) magnetron sputtering coating a 6-nm-thick MgF_2 film and a 50-nm-thick Au film onto the CdSe nanobelts; (iv) focused ion beam (FIB) etching to create two parallel rectangular grooves on the already prepared equipartitioned excitation waveguide; (v) coating a 1-μm-thick Au film onto the already prepared structure through magnetron sputtering, ensuring complete filling of the two processed recesses with Au, resulting in two vertical Au mirrors.

3. Results and discussion

Figure 2(a) illustrates the plasmonic nanolaser, consisting of a plasmonic waveguide and two rectangular Au pillars serving as the FP cavity mirrors. The structure comprises a transparent silicon carbide (SiC) substrate, an 18-nm-thick Au layer, a cadmium selenide (CdSe) layer with thickness ranging from 70 nm to 180 nm, two 6-nm-thick magnesium fluoride (MgF_2) gap layers, and a 1-μm-thick Au superstrate. Figure 2(b) displays a clear cross-sectional view of the lay-

ers. We choose Au instead of silver to avoid oxidation-induced losses in the resonant cavity.[19–22] The excitation condition of the plasmonic nanolaser should satisfy $\Gamma_s g_s > \Gamma_m \alpha_m$, where Γ_s and Γ_m represent the optical confinement factors in the gain medium and metal, respectively, g_s is the CdSe gain layer, and α_m is the metal absorption loss. The absorption of metal is as high as 10^6 cm^{-1}, while that of the CdSe gain layer is on the order of 10^4 cm^{-1}. Lasing condition is realized because the light field confinement factor in the CdSe layer is two orders of magnitude greater than that in the metal region. Fluorescence quenching may arise from direct contact between the metal and the gain medium, while an excessively thick spacer layer will inadequately confine the light, resulting in the weakening of the Purcell effect. The 6-nm-thick MgF_2 gap layer enhances the emission rate without quenching fluorescence.

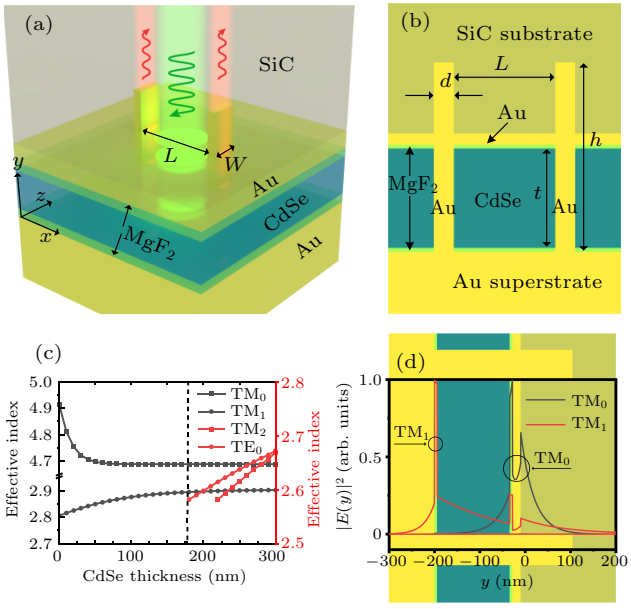


Fig. 2. Proposed plasmon nanolaser design. (a) Schematic diagram of proposed plasmon nanolaser based on an FP cavity composed of two Au mirrors and an Au superstrate/MgF_2/CdSe/MgF_2/Au/SiC substrate structure. (b) Cross-section profile of the FP cavity. The FP cavity has length L, width W, height h, and the CdSe layer thickness t. The thickness of the Au mirror d is fixed at 400 nm. (c) Plots of effective index of the waveguide mode versus t, showing that only two plasmonic modes are not cut off when $t < 180$ nm. (d) Electric field intensity distributions of the plasmonic TM and TM_1 modes along the y direction.

To verify the complete cutoff of optical mode in our designed artificial plasmonic microcavity, we employ mode analysis by using a time-domain finite-difference (FDTD) method. If a significant portion of the mode's energy leaks into the SiC substrate instead of being effectively confined in the plasmonic cavity, the mode is cut off due to excessive losses. Supplementary materials exhibit the energy distributions in different modes at different thickness.TE and TM_2 modes are optical modes that exist inside the CdSe layer, while TM_0 and TM_1 modes are plasmonic modes that propagate along a metal–dielectric surface. The distribution of the mode fields for these modes can be seen in the supplementary materials. In Fig. 2(c), we observe that the photonic modes are cutoff, supporting that only the plasmonic mode exists when the CdSe nanobelt thickness (t) is less than 180 nm, because the SiC substrate has a high index of 2.62. Figure 2(d) shows the strong confinement of plasmonic TM and TM_1 modes in the MgF_2 nanogaps, achieving optical confinements of $\lambda/14$ and $\lambda/15$, respectively. The calculation methods for the optical mode confinements are discussed in the supplementary materials.

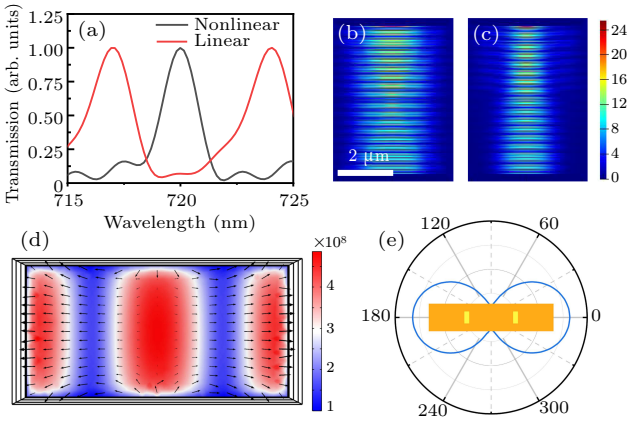


Fig. 3. Simulation analysis of resonant properties for plasmonic TM_1 mode in an FP cavity of $L = 12$ μm and $w = 4$ μm. (a) Calculated resonant spectra for the cavity with self-focusing (black) and without self-focusing effect (red). ((b), (c)) Electric field intensity squared $|E|^2$ distributions (x–z plane) at the resonant wavelengths of (b) 720.1 nm with self-focusing effect and (c) 717.9 nm without self-focusing effect. Scale bar is 2-μm long. (d) Top-view near field numerical simulations of electric field (color map) and oscillation direction (arrow map) based on the proposed MISIM structure. (e) Far-field emission intensity as a function of polarization angle, the polarization angle is defined as the angle included between electric field direction and FP cavity.

The plasmonic mode exhibits a high propagation loss, while the narrow width of FP cavity leads to significant diffraction loss. Therefore, achieving lasing of the plasmonic mode is a challenging task. However, the reduction in diffraction loss resulting from the nonlinear self-focusing effect can assist in lowering the threshold of the plasmonic nanolaser. In this work, we conduct two-dimensional (2D) FDTD simulations to investigate the electric field distribution within the cavity and explore the influence of nonlinear effects on the resonance peaks. The FP cavity dimensions in the simulation are 4 μm in width and 12 μm in length. In Fig. 3(a), the nonlinear case demonstrates narrower resonance peaks for the nonlinear modes. The spectra exhibit an increased Q-factor of 450 and a reduced diffraction loss coefficient α_d of 5595.2 cm^{-1} for the nonlinear peak at 720.1 nm, compared with $Q = 341$ and $\alpha_d = 7428.7$ cm^{-1} for the linear peak at 717.9 nm.[23,24] Figures 3(b) and 3(c) illustrate superior confinement of the fields in the transverse direction (x direction) for the nonlinear cavity compared with that for the linear cavity. The Au mirrors provide a very high reflectivity of 88% for the TM mode and 92%

for the TM_1 mode. These results from the passive cavity qualitatively confirm that the designed cavity effectively mitigates diffraction losses through the nonlinear self-focusing effect. We further investigate the mode-field distribution characteristics and far-field divergence characteristics in our proposed plasmonic nanolaser. Figure 3(d) shows the top-view electric field in the MgF_2 layer of transverse magnetic (TM) mode in the MISIM device. Figure 3(e) exhibits that the electric field in the MgF_2 layer exhibits the strongest coupling to SPP. Therefore the emission is highly polarized along the FP cavity.

To explore the optical properties of our proposed artificial plasmonic nanolaser, we prepare compliant samples based on the designed structure and conduct relevant property measurements. We multiply a 1035-nm picosecond pulsed laser beam and focus it on the sample through a 20-fold objective lens. In the experiment, the pump light is injected from the SiC substrate side and the signal light is collected from the same side. The SEM analysis of the fabricated sample in Fig. 4(a) reveals a clear laminar structure, demonstrating its high quality. Figure 4(b) displays the cavity mirror hole after FIB etching, with sharper edges indicating reduced diffraction loss in the cavity and a lower nanolaser threshold. Figure 4(c) shows an artificial equipartitioned excitation microcavity with dimensions of $L = 12$ μm, $W = 4$ μm, and $d = 400$ nm. The cavity's optical properties vary with pump intensity, exhibiting a threshold of 1.8 GW/cm^2, which is determined by the output spectral linewidth and the kink in the threshold curve. In our proposed structure, the measured light power is approximately 10 μW measured by using a power meter, suggesting a higher intensity than other nanowire lasers. The direction of *xyz* is defined in Fig. 2(a). Since the plasmonic mode is primarily confined in the *x*–*z* plane and the radiation is mainly concentrated in the *x* direction, the laser signal we collect is only a fraction of the plasmonic nanolaser that is reflected by the Au mirror, scattered along the mirror wall in the *y* direction, and collected by the microscope. Consequently, the actual radiation intensity along the *x* direction will be significantly higher. A notch can be introduced to one side of the mirror, and a waveguide can be incorporated in the notch. A 45° reflector can be placed at the end of the waveguide to achieve high efficiency output of the SPP laser. And the SPP laser is advantageous to be collected in *y* direction. To observe the polarization of the nanolaser, a polarizer is added into the measurement optical path while keeping the excitation conditions unchanged. The direction of the polarizer is changed into different polarization directions for observing the pattern and spectrum of the nanolaser by using the CCD and spectrometer. Figures 4(d) and 4(e) present CCD-captured intracavity images at TM and TE, respectively, while figure 4(f) displays intracavity spectral lines for both polarizations, confirming that our nanolaser design operates in the TM polarization. Figure 4(g) demonstrates the emission spectra produced by transitioning from spontaneous emission to amplified spontaneous emission and finally achieving complete laser oscillation as the pump power increases.

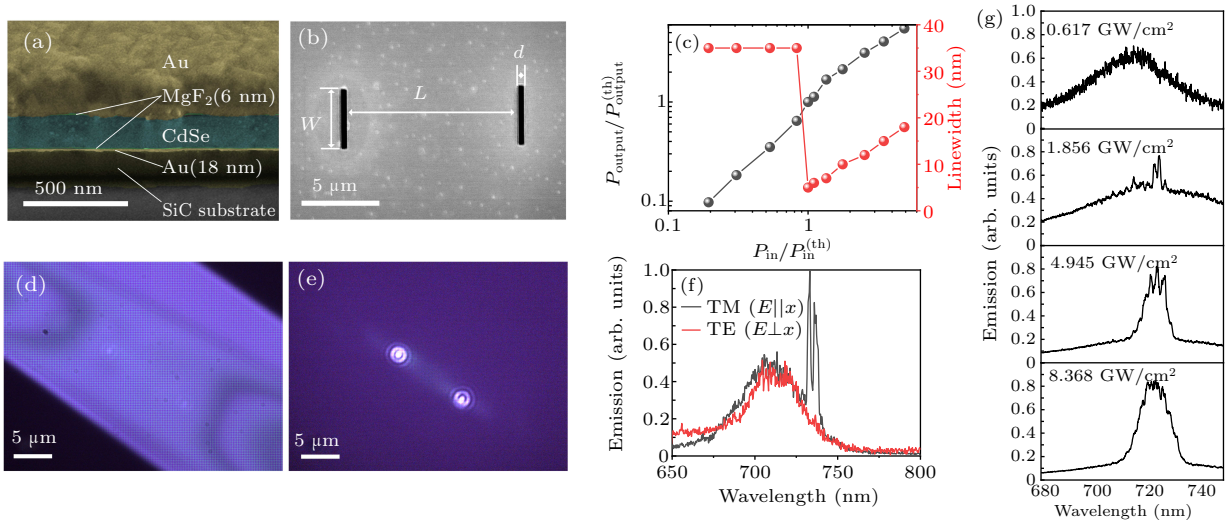


Fig. 4. Optical characterization of proposed plasmonic nanolaser with an FP cavity of $L = 12$ μm. (a) SEM image of cross-section of the as-fabricated plasmonic waveguide. Scale bar is 500-nm long. (b) SEM image of mirror etched with FIB. Scale bar is 5-μm long. (c) Output characteristics of the proposed plasmonic nanolaser. The black and red lines represent the output intensity and linewidth, respectively. ((d), (e)) CCD images in (d) TE (photonic mode) polarization direction and (e) TM (plasmonic mode) polarization direction. (f) Output signals in TE polarization direction (red) and TM polarization direction (black). (g) Emission spectra for the peak pump intensity I_{pump} increasing from 0.617 GW·cm^{-2} to 8.368 GW·cm^{-2}.

We prepare a number of high-quality samples to investigate the influences of structural parameters on the optical properties of our designed artificial plasmonic microcavity. In Fig. 5(a), we observe a blueshift of the nanolaser output's center wavelength as the CdSe nanobelt layer becomes thinner. This blueshift is attributed to the enhanced Purcell effect, which was reported in the literature.[25–27] To maintain a relatively stable thickness of around 130 nm (±10 nm), we

precisely control the growth conditions for CdSe nanobelt. By controlling thickness, we explore the influence of cavity structural parameters on the nanolaser threshold. Figure 5(b) demonstrates that increasing the cavity length of the artificial plasmonic cavity leads the nanolaser threshold to lower. This effect arises from the larger total gain in the cavity for the same power density, resulting in a lower threshold for a given loss. The mirror's reflectivity to the cavity mode slightly increases with thickness, reducing diffraction loss in the cavity. In order to verify the effect of the mirror's thickness on the proposed plasmonic nanolaser's threshold, we design two symmetric FP cavities with mirror thickness of 400 nm and 800 nm, respectively, and an asymmetric FP cavity with mirror thickness of 400 nm and 800 nm on each side respectively. Figure 5(c) reveals that symmetric FP cavity with a mirror thickness of 800 nm has the lowest threshold while symmetric FP cavity with a mirror thickness of 400 nm has a highest threshold. Figure 5(d) shows that increasing the Au mirror length leads the nanolaser threshold to lower, because longer mirrors reduce the transverse diffraction loss of the mode, the threshold decreases. These tunings underscore the remarkable tunability of our designed artificial plasmonic microcavity compared with other natural nanowire cavity,[28,29] showing the superiority of our structure.

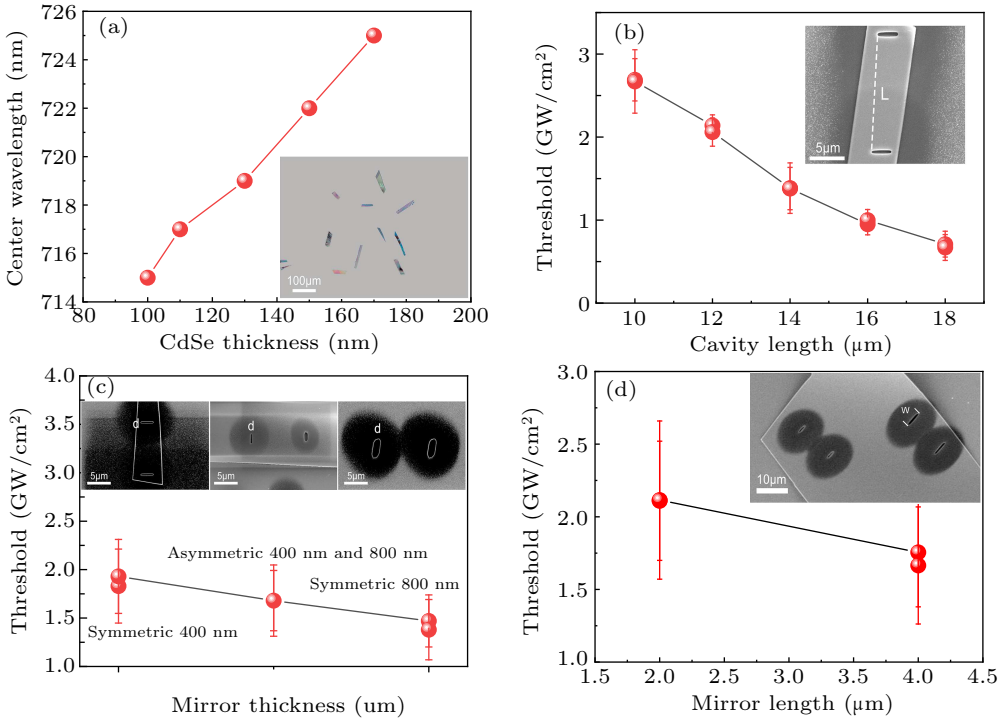


Fig. 5. Center wavelength and threshold versus cavity parameters in the proposed plasmonic nanolaser. (a) Relation between center wavelength of nanolaser spectrum and thickness of the CdSe nanobelt, with center wavelength having a clear blueshift with CdSe nanobelt thickness decreasing. Threshold decreases as (b) cavity length, (c) mirror length, and (d) mirror thickness, respectively.

4. Conclusions

In this work, we present a parameter-tunable artificial plasmonic nanolaser based on the MISIM structure. The proposed cavity achieves a remarkable compression of the mode field volume to $\lambda/14$ and possesses a compact cavity length of only 12 μm, thus the laser feature size can decrease significantly. Compared with natural nanowire lasers, our artificial plasmonic nanolasers provide stronger tuning capabilities in multiple dimensions. Through an exploration of various cavity parameters, we observe that increasing the cavity length, mirror width, and mirror thickness can reduce the nanolaser cavity threshold, providing valuable insights for achieving lower threshold nanolasers. Moreover, we find that thinning the CdSe nanobelt induces the nanolaser's center wavelength to be blue-shifted, which is mainly attributed to exciton–photon strong coupling detuning because of reduced gain layer size. Additionally, the nanolaser output exhibits a wide spectrum width, which is because more longitudinal modes occur with higher pumping. We firmly believe that our designed plasmonic nanolasers hold significant potential applications in the fields of high-quality factor plasmonic nanocavity, sensing, and novel nanolaser light sources.[30–34]

Acknowledgements

Project supported by the National Natural Science Foundation of China (Grant Nos. 12174037, 12204061, 12204030, and 62375003), the Fundamental Research Funds for the Central Universities, China (Grant No. 2022XD-A09), and

the Fund from the State Key Laboratory of Information Photonics and Optical Communication, China (Grant No. IPOC2021ZZ02).

References

[1] Andrae A S and Edler T 2015 *Chanllenges* **6** 117
[2] Miller D A 1997 *Int. J. Optoelectronics* **11** 155
[3] Cerdán L 2021 *Annalen der Physik* **533** 2100122
[4] Sidiropoulos T P, Röder R, Geburt S, Hess O, Maier S A, Ronning C, and Oulton R F 2014 *Nat. Phys.* **10** 870
[5] Altug H, Englund D and Vučković J 2006 *Nat. Phys.* **2** 484
[6] Ma R M and Oulton R F 2019 *Nat. Nanotechnol.* **14** 12
[7] Sidiropoulos T P, Röder R, Geburt S, Hess O, Maier S A, Ronning C and Oulton R F 2014 *Nat. Phys.* **10** 870
[8] Oulton R F, Sorger V J, Zentgraf T, Ma R M, Gladden C, Dai L and Zhang X 2009 *Nature* **461** 629
[9] Hill M T, Marell M, Leong E S, Smalbrugge B, Zhu Y, Sun M and Smit M K 2009 *Opt. Express* **17** 11107
[10] Gao Z, Wang J H, Song P, Kang B, Xu J J and Chen H Y 2020 *Adv. Mater.* **32** 1907233
[11] Temnov V V 2012 *Nat. Photon.* **6** 728
[12] Ni C Y A and Chuang S L 2012 *Opt. Express* **20** 16450
[13] Aust R, Kaul T, Ning C Z, Lingnau B and Lüdge K 2016 *Opt. Quantum Electron.* **48** 1
[14] Liu X, Zhang Q, Xiong Q and Sum T C 2013 *Nano Lett.* **13** 1080
[15] Zhang Q, Shang Q, Shi J, Chen J, Wang R, Mi Y and Sum T C 2017 *ACS Photon.* **4** 2789
[16] Pan A, Zhou W, Leong E S, Liu R, Chin A H, Zou B and Ning C Z 2009 *Nano Lett.* **9** 784
[17] Thanikaikarasan S, Perumal R and Venkatamuthukumar J 2019 *J. Mater. Sci.: Mater. Electron.* **30** 1500
[18] Wang S, Wang W, Lu J P and Ni Z H 2021 *Acta Phys. Sin.* **70** 206802 (in Chinese)
[19] Zhou P, Liang K, Wang Y, Sun Q A, Guo J and Yu L 2023 *Photonics* **10** 69
[20] Wang Y, Li S, Zhang Y and Yu L 2018 *Plasmonics* **13** 107
[21] Rashid K S, Tathfif I, Yaseer A A, Hassan M F and Sagor R H 2021 *Opt. Express* **29** 37541
[22] Khonina S N, Kazanskiy N L, Butt M A, Kaźmierczak A and Piramidowicz R 2021 *Opt. Express* **29** 16584
[23] Ding K, Diaz J O, Bimberg D and Ning C Z 2015 *Laser Photon. Rev.* **9** 488
[24] Merghem K, Akrout A, Martinez A, Aubin G, Ramdane A, Lelarge F and Duan G H 2009 *Appl. Phys. Lett.* **94** 021107
[25] Zhang Q, Li G, Liu X, Qian F, Li Y, Sum T C and ong Q 2014 *Nat. Commun.* **5** 4953
[26] Jiang M, Tang K, Wan P, Xu T, Xu H and Kan C 2021 *Nanoscale* **13** 1663
[27] Du W, Zhang S, Shi J, Chen J, Wu Z, Mi Y and Liu X 2018 *ACS Photon.* **5** 2051
[28] Lu Y J, Wang C Y, Kim J, Chen H Y, Lu M Y, Chen Y C and Gwo S 2014 *Nano Lett.* **14** 4381
[29] Huang C, Sun W, Fan Y, Wang Y, Gao Y, Zhang N and Song Q 2018 *ACS Nano* **12** 3865
[30] Azzam S I, Kildishev A V, Ma R M, Ning C Z, Oulton R, Shalaev V M and Zhang X 2020 *Light: Science & Applications* **9** 90
[31] Stockman M I 2020 *Adv. Photon.* **2** 054002
[32] Ning C Z 2019 *Adv. Photon.* **1** 014002
[33] Keshmarzi E K, Tait R N and Berini P 2018 *Nanoscale* **10** 5914
[34] Zhang Q, Shang Q, Su R, Do T T H and Xiong Q 2021 *Nano Lett.* **21** 1903